Quark and Gluon Momentum Fractions in the Pion from $N_f = 2 + 1 + 1$ Lattice QCD

Constantia Alexandrou,[1,2] Simone Bacchio,[2] Georg Bergner,[3] Jacob Finkenrath,[2] Andrew Gasbarro,[4]
Kyriakos Hadjiyiannakou,[1,2] Karl Jansen,[5] Bartosz Kostrzewa,[6] Konstantin Ottnad,[7] Marcus Petschlies,[8,9] Ferenc Pittler,[2]
Fernanda Steffens,[8,9] Carsten Urbach,[8,9] and Urs Wenger[4,10]

(Extended Twisted Mass Collaboration)

[1]*Department of Physics, University of Cyprus, Nicosia 2109, Cyprus*
[2]*Computation-based Science and Technology Research Center, The Cyprus Institute, Nicosia 2121, Cyprus*
[3]*Institute of Theoretical Physics, Friedrich Schiller University Jena, Jena 07743, Germany*
[4]*Albert Einstein Center, Institute for Theoretical Physics, University of Bern, Bern CH-3012, Switzerland*
[5]*NIC, DESY, Zeuthen 15738, Germany*
[6]*High Performance Computing and Analytics Lab, Rheinische Friedrich-Wilhelms-Universität Bonn, Bonn 53115, Germany*
[7]*PRISMA+ Cluster of Excellence and Institut für Kernphysik, Johannes Gutenberg-Universität Mainz, Mainz 55099, Germany*
[8]*Helmholtz-Institut für Strahlen- und Kernphysik, University of Bonn, Bonn 53115, Germany*
[9]*Bethe Center for Theoretical Physics, University of Bonn, Bonn 53115, Germany*
[10]*Department of Theoretical Physics, CERN, Geneva CH-1211, Switzerland*

We perform the first full decomposition of the pion momentum into its gluon and quark contributions. We employ an ensemble generated by the Extended Twisted Mass Collaboration with $N_f = 2 + 1 + 1$ Wilson twisted mass clover fermions at maximal twist tuned to reproduce the physical pion mass. We present our results in the $\overline{\text{MS}}$ scheme at 2 GeV. We find $\langle x \rangle_{u+d} = 0.601(28)$, $\langle x \rangle_s = 0.059(13)$, $\langle x \rangle_c = 0.019(05)$, and $\langle x \rangle_g = 0.52(11)$ for the separate contributions, respectively, whose sum saturates the momentum sum rule.

Introduction.—Quantum chromodynamics (QCD) manifests itself in the form of a plethora of states—so-called hadrons, formed by quarks and gluons. Pions are particularly interesting hadrons: they are the lightest and simplest of the QCD bound states composed out of quark and antiquark. At the same time pions are also pseudo-Goldstone bosons, with the spontaneous breaking of chiral symmetry playing a fundamental role in the emergence of their mass. Yet, in contrast to the nucleon (proton and neutron), a first principles computation of the pion structure, and in particular how quarks and gluons contribute to its mass and momentum decomposition is still lacking. The importance of this topic is well represented in the Electron Ion Collider (EIC) yellow report [1]: eight main science questions concerning pions (and kaons) are prominently put forward. Let us highlight two of these questions here. What are the quark and gluon energy contributions to the

pion mass, and is the pion full or empty of gluons as viewed at large Q^2? The results presented in this Letter on the momentum decomposition of the pion using lattice QCD simulations address both questions.

As mentioned before, there is a wealth of studies on the nucleon momentum decomposition available in the literature using phenomenological analyses of experimental data [2–5], and, more recently, from precise simulations of lattice QCD at the physical point [6,7]. The reason for the pion being much less well investigated is that proton and neutron structure is experimentally well accessible, while the pion is significantly more challenging because there is no pion target available. For that reason, only recently the first Monte Carlo global QCD analysis for pion parton distribution functions (PDFs) has been presented in Ref. [8], which includes leading neutron electroproduction (LNE) data from HERA and Drell-Yan data from CERN and Fermilab. One of their interesting findings is that the decomposition of the pion momentum $\langle x \rangle_\pi$ into its valence, $\langle x \rangle_v$, sea, $\langle x \rangle_s$, and gluon, $\langle x \rangle_g$ components depends strongly on which data set is included in the analysis. In particular, the inclusion of LNE data, which induce a model dependence in the extraction of the pion PDFs, has a significant effect on the average momentum carried by

gluons and sea quarks in the pion. Precise lattice QCD data for both quark and gluon momentum fractions have, thus, the potential to add new model independent constraints on the extraction of pion PDFs from experimental data. Finally, new data coming from planned EIC experiments, as well as from COMPASS $++$/Amber [9] will help to clarify the quark and gluon dynamics within the pion.

On the theory side one has to resort to models [10,11] or to nonperturbative methods as provided by lattice QCD. Also from the lattice side, there is surprisingly little known for the pion. Most of the computations available so far [12–19] neglect potentially important contributions, the so-called quark-disconnected contributions. Recently, a first computation including disconnected contributions was put forward [20]. Also for the gluon contributions there exists an early computation in the quenched approximation [21], and only one with dynamical fermions at a heavier than physical pion mass [22]. Thus, systematics are certainly not sufficiently controlled. More recently, there are studies using quasidistributions [23–26] and pseudodistributions [27,28] as well as so-called good lattice cross sections [29–31] approaches to compute the x dependence of the pion PDFs directly on the lattice. These studies, however, are restricted to connected contributions only.

In this Letter we present the first calculation of the quark and gluon momentum fractions in the pion based on lattice QCD simulations with $N_f = 2 + 1 + 1$ dynamical quark flavors including all required contributions. The computation is performed using one ensemble with physical values of all four quark mass parameters. This allows us to check the momentum sum rule, i.e., whether all four quark and the gluon fractions sum up to one. This result can pave the way toward a global QCD analysis including experimental data as well as lattice QCD results of the pion, which will help to sort out the discrepancy found between different experimental data sets.

Lattice computation.—Our computation is based on an ensemble [32] generated by the Extended Twisted Mass Collaboration using $N_f = 2 + 1 + 1$ dynamical Wilson twisted mass clover fermions at maximal twist [33,34] and Iwasaki gauge action [35]. With this discretization, lattice artifacts are of $O(a^2)$ only [36]. The lattice volume is $L^3 \times T = 64^3 \times 128$ and the lattice spacing $a = 0.08029(41)$ fm. For strange and charm quarks we use a mixed action approach following Ref. [37], and all quark mass parameters are tuned to assume approximately physical values [32,38]. We give further details on quark mass tuning in the Supplemental Material [39]. For all estimates we used 745 well-separated gauge configurations.

The relevant elements of the traceless Euclidean energy-momentum tensor (EMT) for quark flavor q with the symmetrized covariant derivative $\overleftrightarrow{D}_\mu$ read

$$\bar{T}^q_{\mu\nu} = -\frac{(i)^{\kappa_{\mu\nu}}}{4} \bar{q} \left(\gamma_\mu \overleftrightarrow{D}_\nu + \gamma_\nu \overleftrightarrow{D}_\mu - \delta_{\mu\nu} \frac{1}{2} \gamma_\rho \overleftrightarrow{D}_\rho \right) q, \quad (1)$$

with $\kappa_{\mu\nu} = \delta_{\mu,4}\delta_{\nu,4}$. Analogously for the gluon

$$\bar{T}^g_{\mu\nu} = (i)^{\kappa_{\mu\nu}} \left(F_{\mu\rho}F_{\nu\rho} + F_{\nu\rho}F_{\mu\rho} - \delta_{\mu\nu} \frac{1}{2} F_{\rho\sigma}F_{\rho\sigma} \right). \quad (2)$$

For $X = u, d, s, c, g$, one then obtains $\langle x \rangle^X$ from

$$\langle \pi(\mathbf{p}) | \bar{T}^X_{\mu\nu} | \pi(\mathbf{p}) \rangle = 2\langle x \rangle^X \left(p_\mu p_\nu - \delta_{\mu\nu} \frac{p^2}{4} \right), \quad (3)$$

with on-shell momentum $p = (E_\pi = \sqrt{m_\pi^2 + \mathbf{p}^2}, \mathbf{p})$. We extract these matrix elements from ratios of Euclidean three- and two-point functions

$$R^X_{\mu\nu}(t, t_f, t_i; \mathbf{p}) = \frac{\langle \pi(t_f, \mathbf{p}) \bar{T}^X_{\mu\nu}(t) \pi(t_i, \mathbf{p}) \rangle}{\langle \pi(t_f, \mathbf{p}) \pi(t_i, \mathbf{p}) \rangle}, \quad (4)$$

which are related to the matrix element

$$R^X_{\mu\nu}(t, t_f, t_i; \mathbf{p}) \rightarrow \frac{1}{2E_\pi} \frac{\langle \pi(\mathbf{p}) | \bar{T}^X_{\mu\nu} | \pi(\mathbf{p}) \rangle}{1 + \exp\{-E_\pi[T - 2(t_f - t_i)]\}} \quad (5)$$

for $t_f - t, t - t_i$ (and thus $t_f - t_i$) large enough such that excited state contributions have decayed sufficiently. At the same time $T \gtrsim 2(t_f - t_i)$ should be maintained, otherwise finite size effects become sizable via excited states contaminations. R depends on $t_f - t_i$ and $t - t_i$ only, and in the following we set $t_i = 0$.

According to Eq. (3), $\langle x \rangle$ can be extracted with zero pion momentum from tensor elements with $\mu = \nu$, whereas for $\mu \neq \nu$ nonzero momentum is required. In general, one might expect the signal to be noisier with nonzero momentum, and this is indeed the case for the connected-only contribution. However, due to the fact that for $\mu = \nu$ the signal requires the subtraction of the trace of the EMT, the quark-disconnected and gluon contributions are better determined from the off-diagonal elements of the EMT, see also Ref. [7]. Therefore, we determine the connected-only light contribution to $\langle x \rangle$ from $\bar{T}_{44}$ at zero pion momentum $\mathbf{p} = 0$, and all the other contributions from $\bar{T}_{4k}$ with smallest nonzero momentum $|\mathbf{p}| = 2\pi/L$, averaged over all six spatial directions. Further justification for using (off-) diagonal tensor elements for (dis)connected diagrams is given in Supplemental Material [39].

For the light-quark connected part both two- and three-point functions are constructed using stochastic time-slice sources with spin-color-site components independently and identically distributed, according to $(\mathbb{Z}_2 + i\mathbb{Z}_2)/\sqrt{2}$, with random $\mathbb{Z}_2$ noise and eight stochastic samples per gauge field configuration. For the quark-disconnected part of any quark flavor, as well as the gluon operator part, we employ point-to-all propagators with 200 randomly distributed source points per configuration and full spin-color dilution to estimate the pion two-point function. The light-quark

loop diagrams with covariant derivative insertion are determined based on the combination of low-mode deflation [40] of the Dirac operator with 200 eigenmodes, and hierarchical probing [41] with one stochastic volume source decomposed to coloring distance of eight lattice sites in each spatial direction. Spin-color dilution is also employed. The strange quark is treated with the same hierarchical probing setup, but without deflation. Analogously, for the charm-quark loops we use 12 spin-color diluted volume sources with coloring distance 4 [7]. The gluon field strength tensor in the gluon operator matrix element is computed with the clover field definition, see, e.g., [42]. We apply ten levels of stout smearing [43] to the gauge links in order to sufficiently reduce ultraviolet fluctuations, see Refs. [6,7].

Errors are computed using the bootstrap method with fully correlated fits. Since lattice artifacts are of $\mathcal{O}(a^2)$ with our discretization, we expect discretization errors generically of the size $a^2\Lambda_{\mathrm{QCD}}^2$. For the value of the lattice spacing a used here this amounts to $\sim 2.6\%$ with unknown coefficient.

Renormalization.—The quark flavor-nonsinglet combinations renormalize with Z_{qq} as

$$\langle x \rangle_{u-d}^R = Z_{qq}(\langle x \rangle_u - \langle x \rangle_d),$$
$$\langle x \rangle_{u+d-2s}^R = Z_{qq}(\langle x \rangle_u + \langle x \rangle_d - 2\langle x \rangle_s),$$
$$\langle x \rangle_{u+d+s-3c}^R = Z_{qq}(\langle x \rangle_u + \langle x \rangle_d + \langle x \rangle_s - 3\langle x \rangle_c). \quad (6)$$

For the pion, $\langle x \rangle_{u-d}^R = 0$ in the isospin symmetric case, as simulated here. The quark-singlet and gluon components mix under renormalization according to

$$\begin{pmatrix} \sum_f \langle x \rangle_f^R \\ \langle x \rangle_g^R \end{pmatrix} = \begin{pmatrix} Z_{qq}^s & Z_{qg} \\ Z_{gq} & Z_{gg} \end{pmatrix} \begin{pmatrix} \sum_f \langle x \rangle_f \\ \langle x \rangle_g \end{pmatrix} \quad (7)$$

with Z_{qq}^s the quark-singlet renormalization constant. Defining $\delta Z_{qq} = Z_{qq}^s - Z_{qq}$, one can solve the set of Eqs. (7) for each single flavor and gluon component:

$$\langle x \rangle_f^R = Z_{qq}\langle x \rangle_f + \frac{\delta Z_{qq}}{N_f}\sum_{f'}\langle x \rangle_{f'} + \frac{Z_{qg}}{N_f}\langle x \rangle_g,$$
$$\langle x \rangle_g^R = Z_{gg}\langle x \rangle_g + Z_{gq}\sum_{f'}\langle x \rangle_{f'}. \quad (8)$$

Because of lattice artifacts, renormalization factors are different for $\bar{T}_{\mu\nu}$ with $\mu = \nu$ and $\mu \neq \nu$. The diagonal elements of the renormalization matrix have been determined nonperturbatively and the off-diagonal elements perturbatively in Ref. [7], see also Supplemental Material [39]. Since these mixing coefficients have been determined using one-loop perturbation theory, we do not have an error

estimate available. In order to account for the uncertainty, we perform the computation once including the mixing, and once excluding it, and take the spread as error estimate.

Results.—We compute $R^X(t)$ in Eq. (4) for various values of t_f. Solving Eq. (3) for $\langle x \rangle$ and inserting Eq. (5), we then extract $\langle x \rangle^X(t)$, where X stands for l, conn (with $l \equiv u + d$), l, disc, s, c, and g. For large enough t_f we expect $\langle x \rangle(t)$ to show a plateau for $t - t_f/2$ around 0. Thus, we fit a constant symmetrically around $t - t_f/2 = 0$ with fit range denoted as t_p to our bare data for $\langle x \rangle(t)$ (for plots of this bare data see Supplemental Material [39]). In Fig. 1 we show the result of such constant fits to the light connected contribution as a function of the source sink separation t_f for different values of t_p. Between $t_f = 4.5$ fm and $t_f = 5.14$ fm we see agreement for all values of t_p. For $t_f = 5.78$ fm the results for the smallest three t_p values still agree with the previous ones. However, for the larger t_p values we start to see finite size effects due to $T/2 < t_f$, also visible in the bad χ^2/dof values.

In Fig. 2 we again show the fit results as a function of t_f for different t_p values, but here for the light disconnected and the strange, charm and gluon contributions. For the quark-disconnected contributions we loose the signal for $t_f > 2.25$ fm. However, for all three cases we observe agreement between all results for $1.61 \text{ fm} \leq t_f \leq 2.25 \text{ fm}$, confirming ground state dominance. Thus, we are confident that the final result can be determined in this region of t_f values.

We arrive at the final result by assigning a weight $w = \exp\left(-\frac{1}{2}[\chi^2 - 2\mathrm{dof}]\right)$ to every fit with given χ^2 value and degrees of freedom (dof). Then we take the weighted average (see also [44]) over all constant fits in the aforementioned regions of t_f values. The combined statistical and systematic error is computed by repeating this
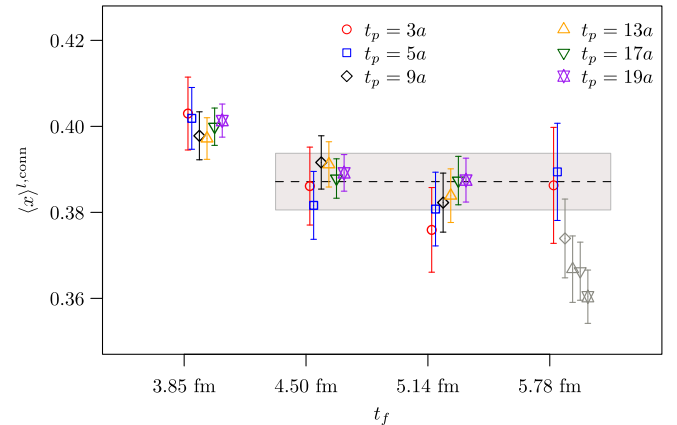

FIG. 1. Fit results for the bare light connected $\langle x \rangle^{l,\mathrm{conn}}$ as a function of t_f for different fit range values t_p. Grayed out points have a $\chi^2/\mathrm{dof} > 1.3$. Gray band and dashed line represent the result and total error obtained via a weighted averaging procedure.
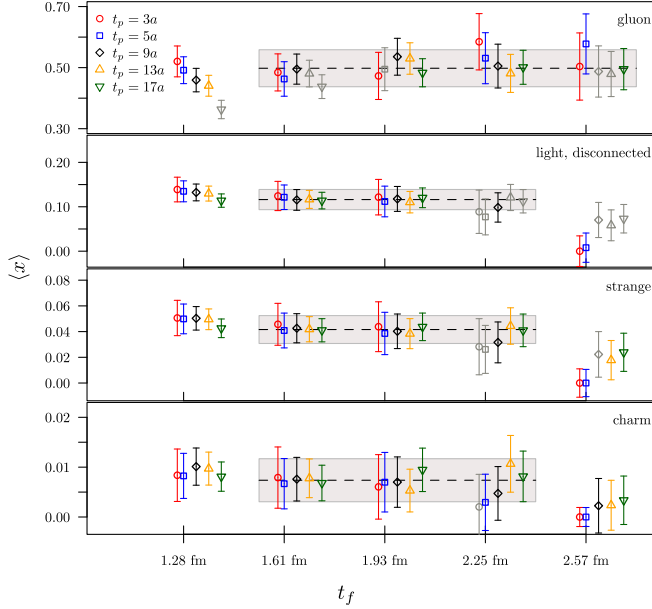
FIG. 2. Fit results for the bare quark disconnected and the gluon $\langle x \rangle$ as a function of t_f for different fit range values t_p. Grayed out points have a $\chi^2/\mathrm{dof} > 1.3$. Gray band and dashed line represent the result and total error obtained via a weighted averaging procedure.

procedure on all bootstrap samples with weights corresponding to the fits on the samples. Alternatively, we have also performed fits which take explicitly into account excited state contaminations again for various t_f and t_p values leading to consistent results, but with a different distribution of statistical and systematic errors.

Using the so-extracted bare values for $\langle x \rangle^X$ (see Supplemental Material [39]), we are now in the position to compute the renormalized flavor nonsinglet and singlet contributions to $\langle x \rangle$. We obtain for the nonsinglet ones from Eq. (6)

$$\langle x \rangle^R_{u+d-2s} = 0.48(1), \qquad \langle x \rangle^R_{u+d+s-3c} = 0.60(3), \quad (9)$$

where we recall that $\langle x \rangle_{u-d} = 0$ due to isospin symmetry in the light-quark sector. For the singlet contributions we find, using Eqs. (7) and (8),

$$\sum_f \langle x \rangle^R_f = 0.68(5)(_{-3}), \qquad \langle x \rangle^R_g = 0.52(11)(^{+2}). \quad (10)$$

The first error represents the combined statistical and fit range uncertainty, the second error comes from the mixing under renormalization. The sum of all contributions amounts to $\langle x \rangle^R_{\mathrm{total}} = 1.20(13)(_{-3})$, compatible with the expected value of 1 within two sigma. This is an important result because, in contrast to phenomenological analyses where the saturation of the momentum sum rule is imposed, in our work such saturation is a result of the computation.
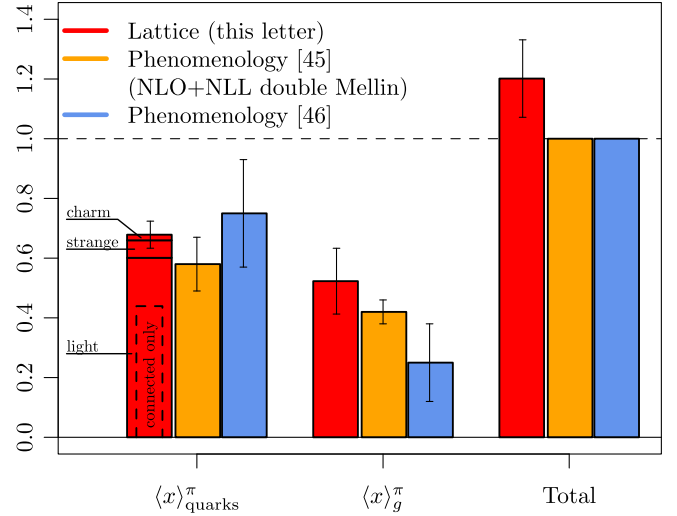

FIG. 3. Comparison to Refs. [45,46] at 2 GeV in the $\overline{\mathrm{MS}}$ scheme. In the two phenomenological computations the momentum sum rule is imposed, at next-to-leading order (NLO) and next-to-leading logarithmic (NLL) accuracy.

In Fig. 3 we compare to the recent phenomenological results from Refs. [45,46]. Our work agrees within errors with these state-of-art phenomenological results.

In Table I we compile all the contributions again and compare to the literature. The only other lattice result was presented in Ref. [20], where $N_f = 2 + 1$ flavor QCD was used and results have been extrapolated to the continuum and the physical point. However, the gluon contribution has not been computed and, thus, the mixing could not be taken into account. Therefore, the comparison of the quark-singlet contributions is of limited meaningfulness. The nonsinglet contribution $\langle x \rangle^R_{u+d-2s}$ is better suited for a comparison. While currently there is a discrepancy between the results, we notice that a full comparison should be attempted only after the inclusion of all unaccounted systematics.

Finally, the results from the momentum sum rule decomposition can be used to determine how quarks and gluons contribute to the pion mass. In principle, mass can be decomposed in QCD in different ways [47–52]. Choosing

TABLE I. Compilation of results and comparison to literature. All values are at 2 GeV in the $\overline{\mathrm{MS}}$ scheme.

	This work	[20]	[45]	[46]
$\langle x \rangle^R_l)$	$0.601(28)(_{-21})$	$\cdots$	$\cdots$	$\cdots$
$\langle x \rangle^R_s$	$0.059(13)(_{-10})$	$\cdots$	$\cdots$	$\cdots$
$\langle x \rangle^R_c$	$0.019(05)(_{-10})$	$\cdots$	$\cdots$	$\cdots$
$\langle x \rangle^R_g$	$0.52(11)(^{+02})$	$\cdots$	$0.42(4)$	$0.25(13)$
$\Sigma_f \langle x \rangle^R_f$	$0.68(05)(_{-03})$	$0.220(207)$	$0.58(9)$	$0.75(18)$
$\langle x \rangle^R_{u+d-2s}$	$0.48(01)$	$0.344(28)$	$\cdots$	$\cdots$
$\langle x \rangle^R_{u+d+s-3c}$	$0.60(03)$	$\cdots$	$\cdots$	$\cdots$

the sum rule of Ref. [52], $M_{\pi,q} = (3M_\pi/4)\langle x\rangle_{\text{quarks}}^R$ and $M_{\pi,g} = (3M_\pi/4)\langle x\rangle_g^R$, which amounts to 70(5) MeV and 55(12) MeV at 2 GeV in the $\overline{\text{MS}}$ scheme, respectively. Note that the gluon contribution is the same in Ji's original mass decomposition [47,48]. The remaining contribution is split among a trace anomaly term and a term proportional to the quark mass.

Summary and outlook.—In this Letter, we have presented results for the complete flavor decomposition of the average momentum of quarks and gluons in the pion for the first time. The computation in $N_f = 2 + 1 + 1$ lattice QCD is performed directly with physical values of the quark mass parameters making an extrapolation to the physical point superfluous and, thus, avoiding any systematic uncertainty from such an extrapolation. However, we work at a single value of the lattice spacing only, which does not allow us to take the continuum limit. Therefore, we have to expect lattice artifacts of $\mathcal{O}(a^2)$ which we cannot account for rigorously. The renormalization constants have been computed nonperturbatively, while the mixing coefficients were computed in perturbation theory.

We find the momentum sum rule to be fulfilled within two sigma errors, see Fig. 3. When comparing to phenomenological determinations from Refs. [45,46] we find reasonable agreement within relatively large uncertainties. Comparing to the only other lattice QCD computation [20] including quark disconnected contributions, but not the mixing and the gluon contribution, we observe a deviation well outside uncertainties.

Future plans include determining $\langle x\rangle$ in the pion for two more lattice spacing values directly at the physical point. Preliminary results for the flavor nonsinglet components at a finer lattice spacing show agreement within errors. Moreover, work is in progress to determine the mixing coefficients nonperturbatively. This work opens the possibility to combine lattice QCD results and experimental data in a global phenomenological analysis.

[1] R. Abdul Khalek *et al.*, Science requirements and detector concepts for the electron-ion collider: EIC yellow report, arXiv:2103.05419.

[2] R. D. Ball *et al.* (NNPDF Collaboration), Parton distributions from high-precision collider data, Eur. Phys. J. C **77,** 663 (2017).

[3] S. Dulat, T.-J. Hou, J. Gao, M. Guzzi, J. Huston, P. Nadolsky, J. Pumplin, C. Schmidt, D. Stump, and C. P. Yuan, New parton distribution functions from a global analysis of quantum chromodynamics, Phys. Rev. D **93,** 033006 (2016).

[4] S. Alekhin, J. Blümlein, S. Moch, and R. Placakyte, Parton distribution functions, α_s, and heavy-quark masses for LHC Run II, Phys. Rev. D **96,** 014011 (2017).

[5] E. Moffat, W. Melnitchouk, T. C. Rogers, and N. Sato [Jefferson Lab Angular Momentum (JAM) Collaboration], Simultaneous Monte Carlo analysis of parton densities and fragmentation functions, Phys. Rev. D **104,** 016015 (2021).

[6] C. Alexandrou, M. Constantinou, K. Hadjiyiannakou, K. Jansen, C. Kallidonis, G. Koutsou, A. V. Avilés-Casco, and C. Wiese, Nucleon Spin, and Momentum Decomposition Using Lattice QCD Simulations, Phys. Rev. Lett. **119,** 142002 (2017).

[7] C. Alexandrou, S. Bacchio, M. Constantinou, J. Finkenrath, K. Hadjiyiannakou, K. Jansen, G. Koutsou, H. Panagopoulos, and G. Spanoudes, Complete flavor decomposition of the spin and momentum fraction of the proton using lattice QCD simulations at physical pion mass, Phys. Rev. D **101,** 094513 (2020).

[8] P. C. Barry, N. Sato, W. Melnitchouk, and C.-R. Ji, First Monte Carlo Global QCD Analysis of Pion Parton Distributions, Phys. Rev. Lett. **121,** 152001 (2018).

[9] B. Adams *et al.*, Letter of intent: A new QCD facility at the $M2$ beam line of the CERN SPS (COMPASS++/AMBER), arXiv:1808.00848.

[10] M. Ding, K. Raya, D. Binosi, L. Chang, C. D. Roberts, and S. M. Schmidt, Symmetry, symmetry breaking, and pion parton distributions, Phys. Rev. D **101,** 054014 (2020).

[11] A. Freese, I. C. Cloët, and P. C. Tandy, Gluon PDF from quark dressing in the nucleon and pion, arXiv:2103.05839.

[12] G. Martinelli and C. T. Sachrajda, Pion structure functions from lattice QCD, Phys. Lett. B **196,** 184 (1987).

[13] C. Best, M. Göckeler, R. Horsley, E.-M. Ilgenfritz, H. Perlt, P. E. L. Rakow, A. Schäfer, G. Schierholz, A. Schiller, and S. Schramm, Pion and rho structure functions from lattice QCD, Phys. Rev. D 56, 2743 (1997).

[14] M. Guagnelli, K. Jansen, F. Palombi, R. Petronzio, A. Shindler, and I. Wetzorke (Zeuthen-Rome (ZeRo) Collaboration), Non-perturbative pion matrix element of a twist-2 operator from the lattice, Eur. Phys. J. C 40, 69 (2005).

[15] S. Capitani, K. Jansen, M. Papinutto, A. Shindler, C. Urbach, and I. Wetzorke, Parton distribution functions with twisted mass fermions, Phys. Lett. B 639, 520 (2006).

[16] A. Abdel-Rehim et al., Nucleon and pion structure with lattice QCD simulations at physical value of the pion mass, Phys. Rev. D 92, 114513 (2015); Erratum, Phys. Rev. D 93, 039904 (2016).

[17] M. Oehm, C. Alexandrou, M. Constantinou, K. Jansen, G. Koutsou, B. Kostrzewa, F. Steffens, C. Urbach, and S. Zafeiropoulos, $\langle x \rangle$ and $\langle x^2 \rangle$ of the pion PDF from lattice QCD with $N_f = 2 + 1 + 1$ dynamical quark flavors, Phys. Rev. D 99, 014508 (2019).

[18] C. Alexandrou, S. Bacchio, I. Cloet, M. Constantinou, K. Hadjiyiannakou, G. Koutsou, and C. Lauer (ETM Collaboration), Mellin moments $\langle x \rangle$ and $\langle x^2 \rangle$ for the pion and kaon from lattice QCD, Phys. Rev. D 103, 014508 (2021).

[19] C. Alexandrou, S. Bacchio, I. Cloët, M. Constantinou, K. Hadjiyiannakou, G. Koutsou, and C. Lauer (ETM Collaboration), Pion and kaon $\langle x^3 \rangle$ from lattice QCD and PDF reconstruction from Mellin moments, Phys. Rev. D 104, 054504 (2021).

[20] M. Löffler, D. Jenkins, R. Rödl, A. Schäfer, L. Walter, P. Wein, S. Weishäupl, and T. Wurm (RQCD Collaboration), Mellin moments of spin dependent and independent PDFs of the ρ and π, arXiv:2108.07544.

[21] H. B. Meyer and J. W. Negele, Gluon contributions to the pion mass and light cone momentum fraction, Phys. Rev. D 77, 037501 (2008).

[22] P. E. Shanahan and W. Detmold, Gluon gravitational form factors of the nucleon and the pion from lattice QCD, Phys. Rev. D 99, 014511 (2019).

[23] X. Ji, Parton Physics on a Euclidean Lattice, Phys. Rev. Lett. 110, 262002 (2013).

[24] J.-H. Zhang, J.-W. Chen, L. Jin, H.-W. Lin, A. Schäfer, and Y. Zhao, First direct lattice-QCD calculation of the x-dependence of the pion parton distribution function, Phys. Rev. D 100, 034505 (2019).

[25] H.-W. Lin, J.-W. Chen, Z. Fan, J.-H. Zhang, and R. Zhang, Valence-quark distribution of the kaon and pion from lattice QCD, Phys. Rev. D 103, 014516 (2021).

[26] X. Gao, L. Jin, C. Kallidonis, N. Karthik, S. Mukherjee, P. Petreczky, C. Shugert, S. Syritsyn, and Y. Zhao, Valence parton distribution of the pion from lattice QCD: Approaching the continuum limit, Phys. Rev. D 102, 094513 (2020).

[27] A. V. Radyushkin, Quasi-parton distribution functions, momentum distributions, and pseudo-parton distribution functions, Phys. Rev. D 96, 034025 (2017).

[28] B. Joó, J. Karpie, K. Orginos, A. V. Radyushkin, D. G. Richards, R. S. Sufian, and S. Zafeiropoulos, Pion valence structure from Ioffe-time parton pseudodistribution functions, Phys. Rev. D 100, 114512 (2019).

[29] Y.-Q. Ma and J.-W. Qiu, Exploring Partonic Structure of Hadrons Using ab initio Lattice QCD Calculations, Phys. Rev. Lett. 120, 022003 (2018).

[30] R. S. Sufian, J. Karpie, C. Egerer, K. Orginos, J.-W. Qiu, and D. G. Richards, Pion valence quark distribution from matrix element calculated in lattice QCD, Phys. Rev. D 99, 074507 (2019).

[31] R. S. Sufian, C. Egerer, J. Karpie, R. G. Edwards, B. Joó, Y.-Q. Ma, K. Orginos, J.-W. Qiu, and D. G. Richards, Pion valence quark distribution from current-current correlation in lattice QCD, Phys. Rev. D 102, 054508 (2020).

[32] C. Alexandrou et al., Simulating twisted mass fermions at physical light, strange and charm quark masses, Phys. Rev. D 98, 054518 (2018).

[33] R. Frezzotti, P. A. Grassi, S. Sint, and P. Weisz (Alpha Collaboration), Lattice QCD with a chirally twisted mass term, J. High Energy Phys. 08 (2001) 058.

[34] R. Frezzotti and G. C. Rossi, Twisted mass lattice QCD with mass nondegenerate quarks, Nucl. Phys. B, Proc. Suppl. 128, 193 (2004).

[35] Y. Iwasaki, Renormalization group analysis of lattice theories and improved lattice action: Two-dimensional nonlinear O(N) sigma model, Nucl. Phys. B258, 141 (1985).

[36] R. Frezzotti and G. C. Rossi, Chirally improving Wilson fermions. 1. O(a) improvement, J. High Energy Phys. 08 (2004) 007.

[37] R. Frezzotti and G. C. Rossi, Chirally improving Wilson fermions. II. Four-quark operators, J. High Energy Phys. 10 (2004) 070.

[38] C. Alexandrou et al., Quark masses using twisted mass fermion gauge ensembles, arXiv:2104.13408.

[39] See Supplemental Material at http://link.aps.org/supplemental/10.1103/PhysRevLett.127.252001 for further discussion of bare lattice data for $\langle x \rangle^l$ and $\langle x \rangle^g$, the applied renormalization procedure and the lattice setup of sea and valence quark action.

[40] A. S. Gambhir, A. Stathopoulos, and K. Orginos, Deflation as a method of variance reduction for estimating the trace of a matrix inverse, SIAM J. Sci. Comput. 39, A532 (2017).

[41] A. Stathopoulos, J. Laeuchli, and K. Orginos, Hierarchical probing for estimating the trace of the matrix inverse on toroidal lattices, arXiv:1302.4018.

[42] K. Jansen and C. Liu, Implementation of Symanzik's improvement program for simulations of dynamical Wilson fermions in lattice QCD, Comput. Phys. Commun. 99, 221 (1997).

[43] C. Morningstar and M. J. Peardon, Analytic smearing of SU(3) link variables in lattice QCD, Phys. Rev. D 69, 054501 (2004).

[44] Sz. Borsanyi et al., Leading hadronic contribution to the muon magnetic moment from lattice QCD, Nature (London) 593, 51 (2021).

[45] P. C. Barry, C.-R. Ji, N. Sato, and W. Melnitchouk, Global QCD analysis of pion parton distributions with threshold resummation, arXiv:2108.05822.

[46] I. Novikov et al., Parton distribution functions of the charged pion within the xFitter framework, Phys. Rev. D 102, 014040 (2020).

[47] X.-D. Ji, A QCD Analysis of the Mass Structure of the Nucleon, Phys. Rev. Lett. **74,** 1071 (1995).

[48] X.-D. Ji, Breakup of hadron masses and energy-momentum tensor of QCD, Phys. Rev. D **52,** 271 (1995).

[49] C. Lorcé, On the hadron mass decomposition, Eur. Phys. J. C **78,** 120 (2018).

[50] Y. Hatta, A. Rajan, and K. Tanaka, Quark and gluon contributions to the QCD trace anomaly, J. High Energy Phys. 12 (2018) 008.

[51] K. Tanaka, Three-loop formula for quark and gluon contributions to the QCD trace anomaly, J. High Energy Phys. 01 (2019) 120.

[52] A. Metz, B. Pasquini, and S. Rodini, Revisiting the proton mass decomposition, Phys. Rev. D **102,** 114042 (2020).

[53] http://www.gauss-centre.eu.

[54] Jülich Supercomputing Centre, JUQUEEN: IBM blue Gene/Q supercomputer system at the Jülich supercomputing centre, J. Large-Scale Res. Facil. **1,** A1 (2015).

[55] Jülich Supercomputing Centre, JURECA: Modular supercomputer at Jülich Supercomputing Centre, J. Large-Scale Res. Facil. **4,** A132 (2018).

[56] Jülich Supercomputing Centre, JUWELS: Modular Tier-0/1 Supercomputer at the Jülich Supercomputing Centre, J. Large-Scale Res. Facil. **5,** A135 (2019).

[57] K. Jansen and C. Urbach, tmLQCD: A program suite to simulate Wilson twisted mass lattice QCD, Comput. Phys. Commun. **180,** 2717 (2009).

[58] A. Abdel-Rehim, F. Burger, A. Deuzeman, K. Jansen, B. Kostrzewa, L. Scorzato, and C. Urbach, Recent developments in the tmLQCD software suite, Proc. Sci., LATTICE2013 (**2014**) 414.

[59] A. Deuzeman, K. Jansen, B. Kostrzewa, and C. Urbach, Experiences with OpenMP in tmLQCD, Proc. Sci., LATTICE2013 (**2013**) 416 [arXiv:1311.4521].

[60] A. Deuzeman, S. Reker, and C. Urbach (ETM Collaboration), Lemon: An MPI parallel I/O library for data encapsulation using LIME, Comput. Phys. Commun. **183,** 1321 (2012).

[61] M. A. Clark, R. Babich, K. Barros, R. C. Brower, and C. Rebbi, Solving lattice QCD systems of equations using mixed precision solvers on GPUs, Comput. Phys. Commun. **181,** 1517 (2010).

[62] R. Babich, M. A. Clark, B. Joo, G. Shi, R. C. Brower, and S. Gottlieb, Scaling lattice QCD beyond 100 GPUs, in *SC11 International Conference for High Performance Computing, Networking, Storage and Analysis Seattle, Washington, 2011* (2011) [arXiv:1109.2935].

[63] M. A. Clark, B. Joó, A. Strelchenko, M. Cheng, A. Gambhir, and R. Brower, Accelerating lattice QCD multigrid on GPUs using fine-grained parallelization, arXiv:1612.07873.

[64] R Core Team, *R: A Language and Environment for Statistical Computing*, R Foundation for Statistical Computing, Vienna, Austria (2019).

[65] B. Kostrzewa, J. Ostmeyer, M. Ueding, and C. Urbach, hadron: Package to extract hadronic quantities, https://github.com/HISKP-LQCD/hadron (2020), R package version 3.0.1.